Non-specific effects of the CINNAMATE-4-HYDROXYLASE inhibitor piperonylic acid

Ilias El Houari[a,b], Petr Klíma[c], Alexandra Baekelandt[a,b], Paul E. Staswick[d], Veselina Uzunova[e], Charo I. Del Genio[f], Ward Steenackers[a,b], Petre I. Dobrev[c], Roberta Filepová[c], Ondrej Novák[g], Richard Napier[e], Jan Petrášek[c,h], Dirk Inzé[a,b], Wout Boerjan[a,b], Bartel Vanholme[a,b*]

[a]Ghent University, Department of Plant Biotechnology and Bioinformatics, Technologiepark 71, B-9052 Ghent, Belgium [b]VIB Center for Plant Systems Biology, Technologiepark 71, B-9052 Ghent, Belgium [c]The Czech Academy of Sciences, Institute of Experimental Botany, Rozvojová 263, 165 02 Prague 6, Czech Republic [d]Department of Agronomy and Horticulture, University of Nebraska–Lincoln, Lincoln, NE, USA [e]School of Life Sciences, University of Warwick, Coventry, CV4 7AL, United Kingdom [f]Centre for Fluid and Complex Systems, School of Computing, Electronics and Mathematics, Coventry University, Prior Street, Coventry CV1 5FB, UK [g]Laboratory of Growth Regulators, Faculty of Science of Palacký University & Institute of Experimental Botany of the Czech Academy of Sciences, Šlechtitelů 27, CZ-78371 Olomouc, Czech Republic [h]Department of Experimental Plant Biology, Faculty of Science, Charles University, Viničná 5, 128 43 Prague 2, Czech Republic

AUTHOR CONTRIBUTIONS

I.E.H., P.K., A.B., P.S., O.N., R.N., J.P., D.I., W.B. and B.V. designed the experiments. I.E.H., P.K., A.B., P.S., V.U., C.D.G., W.S., P.I.D., R.F. and O.N. performed the experiments. R.N., J.P., D.I., W.B. and B.V. supervised the experiments. I.E.H. and B.V. wrote the manuscript with input and contribution from all other authors. B.V. agrees to serve as corresponding author.

Corresponding Author: Bartel Vanholme (Bartel.vanholme@ugent.be).

ABSTRACT

Chemical inhibitors are often implemented for the functional characterization of genes to overcome the limitations associated with genetic approaches. Although it is well established that the specificity of the compound is key to success of a pharmacological approach, off-target effects are often overlooked or simply neglected in a complex biological setting. Here we illustrate the cause and implications of such secondary effects by focusing on piperonylic acid (PA), an inhibitor of CINNAMATE-4-HYDROXYLASE (C4H) that is frequently used to investigate the involvement of lignin during plant growth and development. When supplied to plants, we found that PA is recognized as a substrate by GRETCHEN HAGEN 3.6 (GH3.6), an amido synthetase involved in the formation of the indole-3-acetic acid (IAA) conjugate IAA-Asp. By competing for the same enzyme, PA interferes with IAA conjugation, resulting in an increase in IAA concentrations in the plant. In line with the broad substrate specificity of the GH3 family of enzymes, treatment with PA increased not only IAA levels but also those of other GH3-conjugated phytohormones, namely jasmonic and salicylic acid. Finally, we found that interference with the endogenous function of GH3s potentially contributes to phenotypes previously observed upon PA-treatment. We conclude that deregulation of phytohormone homeostasis by surrogate occupation of the conjugation machinery in the plant is likely a general phenomenon when using chemical inhibitors. Our results hereby provide a novel and important basis for future reference in studies using chemical inhibitors.

INTRODUCTION

Unraveling the physiological function of genes is challenging and a frequent strategy towards this goal is the use of loss-of-function mutants. Such strategies however come with limitations. Due to gene redundancy or compensation mechanisms phenotypes can be masked and if lethal phenotypes are obtained further analysis of the mutants is impossible (Bouche and Bouchez, 2001, Rohde *et al.*, 2004, El Houari *et al.*, 2021b). An alternative approach is to use chemical inhibitors to interfere with the protein of interest and mimic loss-of-function mutants. These inhibitors work rapidly, their treatment is often reversible and they can be applied at a concentration and developmental time-point of interest, thereby circumventing problems related to lethality (McCourt and Desveaux, 2010). In addition, gene redundancy is less of an issue, as inhibitors often target related proteins, allowing simultaneous inactivation of different members of a gene family (Park *et al.*, 2009). On the other hand, this lack of specificity is often considered a drawback of pharmacological approaches, as it could come with unwanted off-target effects (Bain *et al.*, 2007, Karaman *et al.*, 2008). For example triiodobenzoic acid (TIBA), which is used to study polar indole-3-acetic acid (IAA) transport through inhibition of the IAA efflux carrier PIN1 (Geldner *et al.*, 2001), was found to also perturb the plasma membrane proton-motive force (Dindas *et al.*, 2020). In addition, aminoethoxyvinylglycine (AVG), an inhibitor of ethylene biosynthesis (Hanson and Kende, 1976, Najeeb *et al.*, 2015), also inhibits IAA biosynthesis (Soeno *et al.*, 2010). Whereas such off-target effects can have a great impact on data interpretation, they are often only discovered after many years of research.

Piperonylic acid (PA) is a well-known inhibitor of CINNAMATE-4-HYDROXYLASE (C4H; (Schalk *et al.*, 1998, Van de Wouwer *et al.*, 2016, Desmedt *et al.*, 2021, El Houari *et al.*, 2021b) that is often used to demonstrate the involvement of the phenylpropanoid pathway in distinct developmental and physiological plant processes (Naseer *et al.*, 2012, Lee *et al.*, 2013, Reyt *et al.*, 2020). We previously used PA to investigate the role of phenylpropanoid-derived lignin in seedling development (El Houari *et al.*, 2021b), and demonstrated that PA-treated seedlings phenocopy a *c4h-4* mutant by showing an accumulation of adventitious roots (ARs) in the top part of the hypocotyl. This apical accumulation of ARs upon blocking C4H was found to be caused by an inhibition of IAA transport. In this follow-up study we demonstrate that PA is recognized as a substrate by GRETCHEN HAGEN 3.6 (GH3.6), an enzyme involved in the inactivation of IAA. By competing for the same enzyme, PA interferes with the conjugation of IAA, resulting in increased free IAA concentrations in the plant. Using PA as a case study we expose potential risks when treating plants with exogenous molecules to study plant biology, as their conjugation could effectively deregulate phytohormone homeostasis. Hereby we provide a new model for potential broad off-target effects when treating plants with exogenous molecules and inhibitors.

RESULTS

The *c4h-4* mutant and PA-treated seedlings show metabolic differences

In the model plant *Arabidopsis thaliana* CINNAMATE-4-HYDROXYLASE (C4H) is encoded by a single copy gene (El Houari *et al.*, 2021b). As redundancy is not at play for this gene, similar metabolic profiles are expected for *c4h* knockout mutants and plants treated with PA, a well-known C4H inhibitor (Schalk *et al.*, 1998, El Houari *et al.*, 2021b). To assess this, we reevaluated a previously reported metabolic profiling

of etiolated mock-treated Col-0, PA-treated Col-0 and *c4h-4* mutant seedlings transferred to the light for 7 days (El Houari *et al.*, 2021b), now solely comparing the metabolic profiles obtained from *c4h-4* mutants and PA-treated seedlings. PCA analysis showed the formation of two separate clusters (Fig. 1A), pinpointing some metabolic differences between the two conditions. The most evident explanation for this difference is the presence of PA itself, as PA was not supplied to the *c4h-4* mutants. A total of 398 statistically significant differentially abundant compounds were detected between the *c4h-4* mutant and PA-treated seedlings ($p<0.0001$). To further investigate the cause of this difference we assessed the top 15 of differentials between both conditions (Table 1, Fig. S1). All 15 compounds were present in the PA-treated samples but nearly entirely absent in the *c4h-4* mutant. Out of this list, eight could be characterized and these were all either free PA or PA-conjugates (Table 1). The highest differentially accumulating compounds were the amino acid conjugates PA-Asp and PA-Glu, with the detected quantity of PA-Asp being higher than that of all 14 other top differential compounds combined. Noteworthy was also the lower amount of free PA detected compared to its conjugates, reflecting, in accordance to previously reported data (Desmedt *et al.*, 2021), a strong detoxification of PA by the plant.

PA is conjugated to Asp by GH3.6

The conjugation of metabolites to amino acids in plants is conducted by the GH3 protein family (Staswick *et al.*, 2005) and is key in the homeostasis of phytohormones and other bioactive molecules. Among these, the GH3.6-mediated conjugation of IAA to Asp, Ala, Phe and Trp is one of the best documented processes (Staswick *et al.*, 2005). Intriguingly, PA and IAA are similar in size (166 and 175 Da, respectively) and both molecules consist of a planar aromatic carbon skeleton and a side chain

127 containing a carboxylic acid (Fig. 1B). Despite these similarities, both compounds have
128 a different core carbon skeleton, PA being a benzodioxane whereas IAA is an indole.
129 Additionally, the length of the side chains differs for both compounds. However,
130 considering the general substrate promiscuity of the GH3s (Staswick *et al.*, 2005), it is
131 not unlikely that PA could also be recognized by GH3.6 as a substrate. To predict
132 whether binding of PA to GH3.6 is possible and to estimate the likelihood of such an
133 event, we performed an *in silico* docking experiment using PA as well as IAA as
134 substrates (Fig. 1C). As the structure of GH3.6 has not yet been solved, we did a
135 comparative modelling using the crystal structure of GH3.5 as a template. Since GH3.6
136 is expected to have the same two-step catalytic mechanism as GH3.5 (Westfall *et al.*,
137 2016), we retained adenosine monophosphate (AMP) within our model. Docking
138 results of the best predicted binding pose for the natural ligand IAA on the modeled
139 GH3.6 structure showed an excellent correspondence with the binding pose adopted
140 by IAA within the original crystal structure (Fig. 1C, left panel). This suggests that the
141 binding of IAA onto GH3.6 is indeed very likely to happen via the same interactions as
142 in GH3.5. A comparison of this result with the docked poses of PA revealed the
143 occurrence of a bound pose almost identical to that of IAA (Fig. 1C, right panel). This
144 indicates that PA could be a strong ligand for GH3s. To gain empirical evidence that
145 PA can indeed be conjugated by GH3.6, we evaluated the conjugation of PA by GH3.6
146 *in vitro* (Fig. 1D). GH3.6 was fed *in vitro* with different substrates, and the products of
147 the reaction were detected via TLC. A standard for PA-Asp was also included. As a
148 control we provided GH3.6 with either IAA alone, which yielded only IAA, or IAA and
149 Asp, which yielded both IAA and IAA-Asp. Similarly, feeding GH3.6 with PA yielded
150 only PA whereas feeding GH3.6 with PA and Asp resulted in the formation of the PA-

Asp conjugation product. This demonstrates that PA can indeed be conjugated to Asp by GH3.6 *in vitro*.

Conjugation of PA impacts phytohormone homeostasis

Having shown that GH3.6 conjugates PA to Asp, we speculated that high PA levels could overload the conjugation machinery of the plant and thus obstruct the conjugation of IAA. To verify this model, we assessed whether PA treatment could specifically interfere with the conjugation of IAA to Asp in a cellular context (Fig. 2A-B, Table S2). For this purpose, IAA and IAA-conjugate concentrations were measured upon 1, 10, 20 and 60 minutes after addition of 20 nM ^{3}H-IAA with or without 50 µM PA in BY-2 cell cultures. Whereas the mock-treated samples showed a clear decrease in the relative levels of IAA over time, PA-treated samples did not. Conform to these results, mock-treated samples showed an increase in the relative levels of both glycosylated and Asp-conjugated products, whereas such an increase was less pronounced in PA-treated samples. In addition, interesting to note is that the contribution of IAA-Asp to the pool of IAA conjugates seemed to be minor in comparison to the IAA glycosyl esters (Fig. 2A-B, Table S2).

We next verified whether treatment with PA would also result in an increase in IAA levels in Arabidopsis seedlings due to an interference with IAA conjugation. For this purpose, we measured the levels of both IAA and IAA-Asp in etiolated mock- and PA-treated Col-0 seedlings after transfer to the light for 7 days. We indeed observed an increase in IAA-levels of more than 3-fold (Fig. 2C). However, the levels of IAA-Asp were also significantly increased (Fig. 2D), potentially due to a feedback response of the plant to cope with the increased levels of IAA. Alternatively, *GH3* expression could be upregulated in response to the high levels of PA or due to the accumulation of

intermediates upstream of C4H. To assess this, we quantified the shift in expression of IAA-conjugating *GH3* genes in mock- or PA-treated seedlings (Fig. 2E; (Staswick *et al.*, 2005)). Of the six *GH3* genes tested, five showed a significant upregulation upon PA treatment (i.e. *GH3.1*, *GH3.2*, *GH3.3*, *GH3.5* and *GH3.6*). This upregulation in *GH3* expression could explain the increased levels of IAA-Asp.

The conjugation of endogenous plant hormones by GH3s has not only been described for IAA but also for other phytohormones, namely jasmonate (JA) and salicylic acid (SA) (Zhang *et al.*, 2007, Ding *et al.*, 2008, Westfall *et al.*, 2016, Casanova-Saez and Voss, 2019). We thus verified whether treatment of plants with PA would not only increase levels of IAA but also JA and SA levels (Fig. 2F). For this purpose, we measured the levels of IAA, JA and SA in etiolated mock- and PA-treated Col-0 seedlings transferred to the light for 7 days. As observed previously, IAA levels were strongly increased in PA-treated seedlings. In addition, conform to our hypothesis, JA and SA levels were increased significantly upon PA treatment, with JA levels showing a fold increase higher than that of IAA. Although we cannot exclude that the increased levels of JA and SA are secondary to the altered IAA homeostasis, these results indicate that the occupation of the plant conjugation machinery by PA has a broad-spectrum effect on hormone levels in the plant.

Obstructing the function of GH3s results in increased adventitious rooting

We next assessed whether interference of PA with IAA conjugation could contribute to visible phenotypes in the plant. For this purpose, we first assessed potential phenotypic differences between PA-treated and *c4h-4* seedlings. Both were previously shown to have a strongly induced AR growth, specifically at the top part of the hypocotyl (El Houari *et al.*, 2021b). However, whereas for the *c4h-4* mutant this

199 went paired with a reduction in ARs in the bottom part, PA-treated seedlings did not
200 show such a reduction. To see whether this phenotype is dose-dependent, we
201 investigated AR growth in *c4h-4* seedlings and seedlings treated with a concentration
202 range of PA (0-200 μM; Fig. 3A) after etiolation and transfer to the light for 7 days. ARs
203 were quantified while also considering their localization on the hypocotyl, being either
204 at the top third part or the bottom two thirds part. PA-treated seedlings showed a clear
205 apical increase in ARs compared to mock-treatment, with no significant decrease in
206 ARs in the bottom two thirds for any of the concentrations tested (Fig. 3A). The total
207 number of ARs was lower for concentrations 100-200 μM PA than for 25 and 50 μM
208 PA, likely due to toxicity of the high concentrations of PA to the plant. On the other
209 hand, the *c4h-4* mutant showed a significant apical increase of ARs but a near
210 complete depletion of ARs in the bottom two thirds part of the hypocotyl (Fig. 3A).

211 The apical shift in ARs upon blocking C4H is caused by an impaired IAA
212 transport, leading to an apical accumulation and basal depletion in IAA levels (El
213 Houari *et al.*, 2021b). Whereas the *c4h-4* mutant shows a near complete basal
214 depletion in ARs, a small, non-significant reduction in ARs in this region was only
215 visible for high, likely toxic concentrations of PA. We hypothesized that in PA-treated
216 seedlings obstruction of GH3 function by PA leads to a local increase in IAA levels,
217 hereby allowing for basal AR growth. To assess whether obstruction of GH3s by PA
218 could indeed impact AR growth we compared AR growth in mock- and PA-treated Col-
219 0 seedlings to a sextuple *gh3* mutant (Fig. 3B-C). This mutant bears knockouts for the
220 same *GH3* genes whose expression we previously assessed (*gh3.1-6*). As before, PA-
221 treated Col-0 seedlings displayed a strong increase in total ARs compared to the mock-
222 treated Col-0 plants and this increase was specifically situated at the top part of the

hypocotyl. Correspondingly, the *gh3* sextuple mutants also showed a strong induction of ARs compared to the mock-treated Col-0 plants (Fig. 3B-C), albeit along the entirety of the hypocotyl. These results demonstrate that prohibiting GH3-mediated conjugation of IAA upon PA-treatment is likely to contribute to an overall increase in AR growth proliferation.

DISCUSSION

Plants make extensive use of bioactive molecules to steer their growth and development. As these molecules can negatively affect plant growth when mislocalized or when over or under abundant, their levels are under tight control. Accordingly, plants are equipped with a range of enzymes that mediate the conjugation and/or sequestration of these compounds, such as UDP-glycosyltransferases (UGTs), glutathione-S-transferases (GSTs) and amido synthetases (Schröder and Collins, 2002, Casanova-Saez *et al.*, 2021). For example, the glycosylation of several phenylpropanoids allows for the regulation of their endogenous levels via sequestration into the vacuole (Dima *et al.*, 2015, Le Roy *et al.*, 2016), a mechanism which is proposed to mitigate the toxicity of bioactive phenylpropanoid accumulation (Le Roy *et al.*, 2016, Steenackers *et al.*, 2019, Vanholme *et al.*, 2019, El Houari *et al.*, 2021a). Such conjugating enzymes tend to have large substrate promiscuities and can act both on endogenous compounds as well as compounds that are exogenous to the plant (Staswick *et al.*, 2005, Aoi *et al.*, 2020, Mateo-Bonmatí *et al.*, 2021). Consequently, when exogenous compounds are supplied in excess, their inactivation could overwhelm the pool of catabolic enzymes and jeopardize the homeostasis of endogenous bioactive compounds.

In this study we assess potential off-target effects of the C4H inhibitor PA. We confirm previous findings that both PA-treated and *c4h-4* mutant seedlings show an increase of ARs in the top part of the hypocotyl caused by an inhibition in IAA transport (El Houari *et al.*, 2021b). As the apical induction of ARs and inhibition in IAA transport were confirmed in both PA-treated seedlings and *c4h-4* mutant seedlings, we can infer that these phenotypes are indeed caused by the inhibition of C4H. However, here we also demonstrate that GH3.6, an enzyme known to be involved in the conjugation of amino acids to a variety of molecules, recognizes and conjugates PA, resulting in an increase in the levels of free IAA. Although we focused on GH3.6, it is likely that PA is also recognized by other GH3 enzymes and interferes with their normal cellular activity. In addition, glucosyl conjugation products of PA were highly accumulating in PA-treated seedlings and treatment with PA impaired the conjugation of IAA to glucose, likely by also blocking the endogenous function of UGTs. This indicates that also the conjugation of IAA to sugars by UGTs and possibly other classes of conjugating enzymes is impaired by PA.

Besides the PA-mediated increase of endogenous IAA levels, we also demonstrated an increase in the concentration of JA and SA in PA-treated seedlings. As both JA and SA are recognized by GH3s and UGTs (Zhang *et al.*, 2007, Ding *et al.*, 2008, Westfall *et al.*, 2016, Casanova-Saez and Voss, 2019), it is tempting to link the increase in their concentrations upon PA treatment to a mechanism similar to the one described for IAA. However, alternative mechanisms should not be excluded. For example, the increased levels of JA and SA could be secondary to the altered auxin homeostasis. In addition, the PA-mediated increase in SA-levels could be a direct consequence of the inhibition of C4H, as the substrate of C4H (i.e. cinnamic acid) acts

as a precursor of SA (Lefevere *et al.*, 2020, Vlaminck *et al.*, 2022). Considering the critical role of phytohormones in a wide range of plant processes, these findings imply that occupation of the conjugation machinery of the plant by PA could affect a large array of biological processes. Also, and importantly, treatment with other exogenous compounds will likely also obstruct the metabolism of endogenous molecules in a similar manner. Therefore, other chemical inhibitors could, analogously to PA, influence phytohormonal homeostasis by hijacking the plant conjugation machinery. As a consequence, the transcriptome, proteome and metabolome might be altered by such treatment in an indirect manner, causing erroneous conclusions to be drawn. We therefore advise to take into account the catabolism of the exogenous compound by the plant, as this could give valuable insight into possible off-target effects caused by the implemented compound and prohibit confusing primary with secondary effects.

MATERIAL & METHODS

Plant material, transgenic lines, chemicals and growth conditions

Arabidopsis thaliana of the Col-0 ecotype was used for all analyses unless stated otherwise. The *c4h-4* mutant (GK-753B06; (Kleinboelting *et al.*, 2012)) was obtained from the NASC institute. The *gh3* sextuple mutant was obtained from prof. Paul Staswick (Porco *et al.*, 2016). Seeds were vapor-phase sterilized and plants grown on ½ Murashige & Skoog (MS) medium (pH 5.7) containing 2.15 g MS basal salt mixture powder (Duchefa), 10 g sucrose, 0.5 g MES monohydrate, 8 g plant tissue culture agar per liter. When relevant, the medium was supplemented with either dimethyl sulfoxide (DMSO) as a mock treatment or PA (Sigma Aldrich). This compound was prepared as a stock solution in DMSO and was added to the autoclaved medium before pouring the plates. Seeds were stratified using a 2-day cold treatment. To stimulate etiolation,

seeds were given a 4h light pulse and transferred for 7 days to darkness at 21°C. Plates were then transferred to a tissue culture room for 7 days under a 16-h-light/8-h-dark photoperiod at 21°C, after which relevant analyses were conducted.

Metabolic profiling and analysis

For each repeat 8 seedlings were pooled after etiolation and transfer to the light for 7 days. The material was flashfrozen in liquid N_2 and ground using a Retsch mill (1 min, 20 Hz, 5-mm bead). Samples were supplied with 1 mL methanol and incubated for 15 min at 70 °C while shaking at 1000 rpm. Samples were then centrifuged and 800 µL of the supernatant was dried under vacuum. The pellet was dissolved in 100 µL cyclohexane and 100 µL milliQ water was added. After centrifugation 70 µL of the water phase was subjected to UHPLC-MS on an ACQUITY UPLC I-Class system (Waters) consisting of a binary pump, a vacuum degasser, an autosampler, and a column oven. Chromatographic separation was performed on an ACQUITY UPLC BEH C18 (150 × 2.1 mm, 1.7 µm) column (Waters), while maintaining the temperature at 40 °C. A gradient of two buffers (A and B) was utilized: buffer A (99:1:0.1 water:acetonitrile:formic acid, pH 3) and buffer B (99:1:0.1 acetonitrile:water:formic acid, pH 3), as follows: 99% A for 0.1 min decreased to 50% A in 30 min, decreased to 0% from 30 to 40 min. The flow rate was 0.35 mL per min, and the injection volume was 10 µL. This UHPLC system was connected to a Vion IMS QTOF hybrid mass spectrometer (Waters). The LockSpray ion source was used in negative electrospray ionization mode under the following specific conditions: capillary voltage, 3 kV; reference capillary voltage, 2.5 kV; cone voltage, 30 V; source offset, 50 V; source temperature, 120 °C; desolvation gas temperature, 550 °C; desolvation gas flow, 800 liter per h; and cone gas flow, 50 liter per h. The collision energy for full MSe was set at 6 eV (low energy) and ramped from 20 to 70 eV (high energy), intelligent data

capture intensity threshold was set at 5. For DDA-MSMS, the low mass ramp was ramped between 15 and 30 eV. The high mass ramp was ramped between 30 and 70 eV. Nitrogen (greater than 99.5%) was used as desolvation and cone gas. Leucinenkephalin (250 pg per µL solubilized in water:acetonitrile 1:1 (v/v), with 0.1% formic acid) was utilized for the lock mass calibration, with scanning every 2 min at a scan time of 0.1 s. Profile data were recorded through a UNIFI Scientific Information System (Waters). Data processing was performed with Progenesis QI software version 2.4 (Waters). PCA plots were generated using MetaboAnalyst 4.0. To detect significant differential metabolites between the *c4h-4* and PA-treated seedlings we applied several criteria: (1) Peaks should be present in all samples of at least one out of two conditions; (2) Student's t-test $P<0.0001$; (3) average normalized abundance should be higher than 100 counts in at least one out of two conditions; (4) there should be at least a 100-fold difference in peak area between the two conditions. From this set, the 15 most abundant peaks were selected and sorted by detected quantities in PA-treated samples. Annotation of compounds matching these criteria was based on accurate *m/z*, isotope distribution, and tandem mass spectrometry (MS/MS) similarities. Compounds were structurally elucidated based on similarity of their MS/MS spectra with either commercially available standards (PA; Sigma Aldrich) or previously identified metabolites that were already described in the literature (Desmedt *et al.*, 2021).

Homology modelling and docking

To create a putative structure of GH3.6 Modeller 10.1 was used (Sali and Blundell, 1993). Chain B of the crystal structure of AtGH3.5 (PDB: 5KOD) was selected as template, since it has a sequence identity of 91% with AtGH3.6 on an alignment over 573 residues out of 612. Note that of the 39 non-aligned residues, all but 14 were found

at the termini of the protein, where short disordered loops were not crystallized. Sixty-four different initial models were built, performing a slow annealing stage twice on each one. Each model was then refined 16 independent times, specifically targeting the non-aligned region between R376 and A389 to predict its folded state using loop refinement (Fiser *et al.*, 2000). In all the resulting 1024 models, the presence of AMP within the binding site was retained. To identify the best model, each was scored according to a high-resolution version of the Discrete Optimized Protein Energy, or DOPE-HR (Shen and Sali, 2006), and the model with the best score that did not exhibit structural clashes was chosen. All docking runs were performed with Autodock Vina (Vina, 2010). A search space of 7400 cubic Å (20x20x18.5) centered on the binding site (x, y and z coordinates -2.04, 101.2 and 94.73, respectively) was set and a search exhaustiveness of 128 was used. Ligand files were drawn and energy-minimized in Avogadro2 (Hanwell *et al.*, 2012). Ligand files and model were prepared for docking using AutoDockTools (Morris *et al.*, 2009). Docked poses were evaluated visually using IAA as the reference. All visualizations were produced using UCSF Chimera (Pettersen *et al.*, 2004).

Enzyme assays

Conjugation assays were done using GH3.6-GST fusion protein produced in *E. coli* as previously described (Staswick *et al.*, 2005). Qualitative analysis reactions were performed for 16 h at 23°C in 50 mM Tris-HCl, pH 8.6, 1 mM MgCl2, 1 mM ATP, 1 mM DTT, and 2 mM Asp. Either IAA (1 mM) or PA (10 mM) was included in each reaction. Reactions were analyzed on silica gel 60 F260 plates developed in chloroform:ethyl acetate:formic acid (35:55:10, v/v) and then stained with vanillin reagent (6% vanillin [w/v], 1% sulfuric acid [v/v] in ethanol).

Cellular IAA conjugation assays

Cellular ^{3}H-IAA metabolites were determined in tobacco BY-2 cells supplied with 20 nM ^{3}H-IAA (specific activity 25 Ci/mmol, American Radiolabeled Chemicals) and with/without 50 µM PA 48 hours after subcultivation. Samples (50 mg FW) were taken after 1, 10, 20 and 60 minutes of incubation with ^{3}H-IAA. IAA metabolites were extracted and purified according to (Dobrev and Kamınek, 2002) and analyzed on HPLC Ultimate 3000 (Thermo Fisher Scientific, MA, USA) coupled to a radioactivity-HPLC flow detector (Ramona 2000; Raytest, Straubenhardt, Germany) with on-line admixture at volumetric ratio 3:1 of scintillation cocktail Flo-Scint II (Perkin Elmer, MA, USA). Analysis was done on a Kinetex C18 HPLC column (5 µm, 150 mm × 4.6 mm; Phenomenex, Torrance, CA, USA) at 0.6 mL/min with tertiary gradient of A: 400 mM ammonium acetate, pH 4, B: 5% methanol in water by volume, and C: methanol/acetonitrile (1:1, v/v). The gradient program was 5–45% C for 20 min, 45–95% C for 1 min, 95% C for 1 min, with A kept constant at 5%. Metabolite identification was based on comparison of retention times of applied standards.

Phytohormone quantification

For each repeat 40-50 seedlings were pooled after etiolation and transfer to the light for 7 days, with a total of 9 repeats per condition. Samples were frozen and homogenized using a MixerMill (Retsch GmbH). Extraction, purification and detection of phytohormones and their conjugation products (IAA; IAA-Asp; JA; SA) was performed as described previously (Flokova *et al.*, 2014).

RNA isolation and qRT-PCR analysis

Total RNA was isolated from seedlings with TriZol (Invitrogen) after etiolation and transfer to the light for 7 days, purified with the RNeasy Plant Mini Kit (Qiagen) and treated with DNase I (Promega). Complementary DNA (cDNA) was prepared with the

iScript cDNA Synthesis Kit (Bio-Rad) according to the manufacturer's instructions. Relative transcript abundancies were determined using the Roche LightCycler 480 and the LC480 SYBR Green I Master Kit (Roche Diagnostics). The resulting cycle threshold values were converted into relative expression values using the second derivative maximum method. For each of the *GH3* genes *ACTIN2*, *ACTIN7* and *UBIQUITIN10* were used as reference genes for normalization. All experiments were performed in three biological replicates (~10 seedlings per replicate), each with three technical replicates. The primer sequences are listed in Supplemental Table S1.

Adventitious rooting assays

Seedlings were etiolated and transferred to the light for 7 days and the number of ARs was counted separately for the top third part and lower two thirds part along the hypocotyl using a stereomicroscope. The plates were scanned using an Epson Expression 11000XL scanner. Statistical analysis of adventitious rooting was performed using GEE models in the SAS windowing environment (Version 9.4) (El Houari *et al.*, 2021b).

FUNDING INFORMATION

This work was supported by the Fonds voor Wetenschappelijk Onderzoek – Vlaanderen (FWO) through project numbers G008116N and 3G038719 and also by personal grants to IEH by FWO (1S04020N; V414521N), EMBO (STF-8658) and the Belgian American Educational Foundation (BAEF). PS was supported by the University of Nebraska by Agricultural Research Division, funded in part by the USDA. CIDG acknowledges support from UKRI under Future Leaders Fellowship grant number MD/T020652/1. P.K. acknowledges support from the Ministry of Education, Youth, and Sports of the Czech Republic (project no. CZ.02.1.01/0.0/0.0/16_019/0000738, EU Operational Programme “Research, development and education and Centre for Plant Experimental Biology”).

ACKNOWLEDGEMENTS

We would like to thank the VIB Metabolomics Core Facility and Geert Goeminne for processing of the LC-MS samples. We would like to thank Ruben Vanholme and Kris Morreel for help with the analysis of the metabolomics data.

CONFLICT OF INTEREST

The authors declare no conflict of interest.

DATA AVAILABILITY STATEMENT

All relevant data can be found within the manuscript and its supporting materials. To obtain raw data or materials, please contact the corresponding authors.

REFERENCES

Aoi, Y., Hira, H., Hayakawa, Y., Liu, H., Fukui, K., Dai, X., Tanaka, K., Hayashi, K.I., Zhao, Y. and Kasahara, H. (2020) UDP-glucosyltransferase UGT84B1 regulates the levels of indole-3-acetic acid and phenylacetic acid in Arabidopsis. *Biochem Biophys Res Commun*, **532**, 244-250.

Bain, J., Plater, L., Elliott, M., Shpiro, N., Hastie, C.J., Mclauchlan, H., Klevernic, I., Arthur, J.S.C., Alessi, D.R. and Cohen, P.J.B.J. (2007) The selectivity of protein kinase inhibitors: a further update. **408**, 297-315.

Bouche, N. and Bouchez, D. (2001) Arabidopsis gene knockout: phenotypes wanted. *Curr Opin Plant Biol*, **4**, 111-117.

Casanova-Saez, R., Mateo-Bonmati, E. and Ljung, K. (2021) Auxin Metabolism in Plants. *Cold Spring Harb Perspect Biol*, **13**, a039867.

Casanova-Saez, R. and Voss, U. (2019) Auxin Metabolism Controls Developmental Decisions in Land Plants. *Trends Plant Sci*, **24**, 741-754.

Desmedt, W., Jonckheere, W., Nguyen, V.H., Ameye, M., De Zutter, N., De Kock, K., Debode, J., Van Leeuwen, T., Audenaert, K., Vanholme, B. and Kyndt, T. (2021) The phenylpropanoid pathway inhibitor piperonylic acid induces broad-spectrum pest and disease resistance in plants. *Plant Cell Environ*, **44**, 3122-3139.

Dima, O., Morreel, K., Vanholme, B., Kim, H., Ralph, J. and Boerjan, W. (2015) Small glycosylated lignin oligomers are stored in Arabidopsis leaf vacuoles. *Plant Cell*, **27**, 695-710.

Dindas, J., Becker, D., Roelfsema, M.R.G., Scherzer, S., Bennett, M. and Hedrich, R. (2020) Pitfalls in auxin pharmacology. *New Phytol*, **227**, 286-292.

Ding, X., Cao, Y., Huang, L., Zhao, J., Xu, C., Li, X. and Wang, S. (2008) Activation of the indole-3-acetic acid-amido synthetase GH3-8 suppresses expansin expression and promotes salicylate- and jasmonate-independent basal immunity in rice. *Plant Cell*, **20**, 228-240.

Dobrev, P.I. and Kamınek, M.J.J.o.C.A. (2002) Fast and efficient separation of cytokinins from auxin and abscisic acid and their purification using mixed-mode solid-phase extraction. **950**, 21-29.

El Houari, I., Boerjan, W. and Vanholme, B. (2021a) Behind the Scenes: The Impact of Bioactive Phenylpropanoids on the Growth Phenotypes of Arabidopsis Lignin Mutants. *Front Plant Sci*, **12**, 734070.

El Houari, I., Van Beirs, C., Arents, H.E., Han, H., Chanoca, A., Opdenacker, D., Pollier, J., Storme, V., Steenackers, W., Quareshy, M., Napier, R., Beeckman, T., Friml, J., De Rybel, B., Boerjan, W. and Vanholme, B. (2021b) Seedling developmental defects upon blocking CINNAMATE-4-HYDROXYLASE are caused by perturbations in auxin transport. *New Phytol*, **230**, 2275-2291.

Fiser, A., Do, R.K. and Sali, A. (2000) Modeling of loops in protein structures. *Protein Sci*, **9**, 1753-1773.

Flokova, K., Tarkowska, D., Miersch, O., Strnad, M., Wasternack, C. and Novak, O. (2014) UHPLC-MS/MS based target profiling of stress-induced phytohormones. *Phytochemistry*, **105**, 147-157.

Geldner, N., Friml, J., Stierhof, Y.-D., Jürgens, G. and Palme, K. (2001) Auxin transport inhibitors block PIN1 cycling and vesicle trafficking. *Nature*, **413**, 425-428.

Hanson, A.D. and Kende, H. (1976) Biosynthesis of wound ethylene in morning-glory flower tissue. *Plant Physiol*, **57**, 538-541.

Hanwell, M.D., Curtis, D.E., Lonie, D.C., Vandermeersch, T., Zurek, E. and Hutchison, G.R. (2012) Avogadro: an advanced semantic chemical editor, visualization, and analysis platform. *J Cheminform*, **4**, 17.

Karaman, M.W., Herrgard, S., Treiber, D.K., Gallant, P., Atteridge, C.E., Campbell, B.T., Chan, K.W., Ciceri, P., Davis, M.I., Edeen, P.T., Faraoni, R., Floyd, M., Hunt, J.P., Lockhart, D.J., Milanov, Z.V., Morrison, M.J., Pallares, G., Patel, H.K., Pritchard, S., Wodicka, L.M. and Zarrinkar, P.P. (2008) A quantitative analysis of kinase inhibitor selectivity. *Nat Biotechnol*, **26**, 127-132.

Kleinboelting, N., Huep, G., Kloetgen, A., Viehoever, P. and Weisshaar, B. (2012) GABI-Kat SimpleSearch: new features of the Arabidopsis thaliana T-DNA mutant database. *Nucleic Acids Res*, **40**, D1211-1215.

Le Roy, J., Huss, B., Creach, A., Hawkins, S. and Neutelings, G. (2016) Glycosylation is a major regulator of phenylpropanoid availability and biological activity in plants. *Frontiers in plant science*, **7**, 735.

Lee, Y., Rubio, M.C., Alassimone, J. and Geldner, N. (2013) A mechanism for localized lignin deposition in the endodermis. *Cell*, **153**, 402-412.

Lefevere, H., Bauters, L. and Gheysen, G. (2020) Salicylic Acid Biosynthesis in Plants. *Front Plant Sci*, **11**, 338.

Mateo-Bonmatí, E., Casanova-Sáez, R., Šimura, J. and Ljung, K. (2021) Broadening the roles of UDP-glycosyltransferases in auxin homeostasis and plant development. *New Phytologist*, **232**, 642-654.

McCourt, P. and Desveaux, D. (2010) Plant chemical genetics. *New Phytol*, **185**, 15-26.

Morris, G.M., Huey, R., Lindstrom, W., Sanner, M.F., Belew, R.K., Goodsell, D.S. and Olson, A.J. (2009) AutoDock4 and AutoDockTools4: Automated docking with selective receptor flexibility. *J Comput Chem*, **30**, 2785-2791.

Najeeb, U., Atwell, B.J., Bange, M.P. and Tan, D.K.Y. (2015) Aminoethoxyvinylglycine (AVG) ameliorates waterlogging-induced damage in cotton by inhibiting ethylene synthesis and sustaining photosynthetic capacity. *Plant Growth Regulation*, **76**, 83-98.

Naseer, S., Lee, Y., Lapierre, C., Franke, R., Nawrath, C. and Geldner, N. (2012) Casparian strip diffusion barrier in Arabidopsis is made of a lignin polymer without suberin. *Proceedings of the National Academy of Sciences*, **109**, 10101-10106.

Park, S.Y., Fung, P., Nishimura, N., Jensen, D.R., Fujii, H., Zhao, Y., Lumba, S., Santiago, J., Rodrigues, A., Chow, T.F., Alfred, S.E., Bonetta, D., Finkelstein, R., Provart, N.J., Desveaux, D., Rodriguez, P.L., McCourt, P., Zhu, J.K., Schroeder, J.I., Volkman, B.F. and Cutler, S.R. (2009) Abscisic acid inhibits type 2C protein phosphatases via the PYR/PYL family of START proteins. *Science*, **324**, 1068-1071.

Pettersen, E.F., Goddard, T.D., Huang, C.C., Couch, G.S., Greenblatt, D.M., Meng, E.C. and Ferrin, T.E. (2004) UCSF Chimera--a visualization system for exploratory research and analysis. *J Comput Chem*, **25**, 1605-1612.

Porco, S., Pěnčík, A., Rashed, A., Voß, U., Casanova-Sáez, R., Bishopp, A., Golebiowska, A., Bhosale, R., Swarup, R., Swarup, K., Peňáková, P., Novák, O., Staswick, P., Hedden, P., Phillips, A.L., Vissenberg, K., Bennett, M.J. and Ljung, K. (2016) Dioxygenase-encoding AtDAO1 gene controls IAA oxidation and homeostasis in Arabidopsis. *Proceedings of the National Academy of Sciences*, **113**, 11016-11021.

Reyt, G., Chao, Z., Flis, P., Salas-González, I., Castrillo, G., Chao, D.-Y. and Salt, D.E. (2020) Uclacyanin proteins are required for lignified nanodomain formation within casparian strips. *Current Biology*, **30**, 4103-4111. e4106.

Rohde, A., Morreel, K., Ralph, J., Goeminne, G., Hostyn, V., De Rycke, R., Kushnir, S., Van Doorsselaere, J., Joseleau, J.P., Vuylsteke, M., Van Driessche, G., Van Beeumen, J., Messens, E. and Boerjan, W. (2004) Molecular phenotyping of the pal1 and pal2 mutants of Arabidopsis thaliana reveals far-reaching consequences on phenylpropanoid, amino acid, and carbohydrate metabolism. *Plant Cell*, **16**, 2749-2771.

Sali, A. and Blundell, T.L. (1993) Comparative protein modelling by satisfaction of spatial restraints. *J Mol Biol*, **234**, 779-815.

Schalk, M., Cabello-Hurtado, F., Pierrel, M.A., Atanossova, R., Saindrenan, P. and Werck-Reichhart, D. (1998) Piperonylic acid, a selective, mechanism-based inactivator of the trans-cinnamate 4-hydroxylase: A new tool to control the flux of metabolites in the phenylpropanoid pathway. *Plant Physiol*, **118**, 209-218.

Schröder, P. and Collins, C. (2002) Conjugating enzymes involved in xenobiotic metabolism of organic xenobiotics in plants. *International Journal of Phytoremediation*, **4**, 247-265.

Shen, M.Y. and Sali, A. (2006) Statistical potential for assessment and prediction of protein structures. *Protein Sci*, **15**, 2507-2524.

Soeno, K., Goda, H., Ishii, T., Ogura, T., Tachikawa, T., Sasaki, E., Yoshida, S., Fujioka, S., Asami, T. and Shimada, Y. (2010) Auxin biosynthesis inhibitors, identified by a genomics-based approach, provide insights into auxin biosynthesis. *Plant & Cell Physiology*, **51**, 524-536.

Staswick, P.E., Serban, B., Rowe, M., Tiryaki, I., Maldonado, M.T., Maldonado, M.C. and Suza, W. (2005) Characterization of an Arabidopsis enzyme family that conjugates amino acids to indole-3-acetic acid. *The Plant Cell*, **17**, 616-627.

Steenackers, W., El Houari, I., Baekelandt, A., Witvrouw, K., Dhondt, S., Leroux, O., Gonzalez, N., Corneillie, S., Cesarino, I. and Inzé, D. (2019) cis-Cinnamic acid is a natural plant growth-promoting compound. *Journal of experimental botany*, **70**, 6293-6304.

Van de Wouwer, D., Vanholme, R., Decou, R., Goeminne, G., Audenaert, D., Nguyen, L., Hofer, R., Pesquet, E., Vanholme, B. and Boerjan, W. (2016) Chemical Genetics Uncovers Novel Inhibitors of Lignification, Including p-Iodobenzoic Acid Targeting CINNAMATE-4-HYDROXYLASE. *Plant Physiol*, **172**, 198-220.

Vanholme, B., El Houari, I. and Boerjan, W. (2019) Bioactivity: phenylpropanoids' best kept secret. *Curr Opin Biotechnol*, **56**, 156-162.

Vina, A. (2010) Improving the speed and accuracy of docking with a new scoring function, efficient optimization, and multithreading Trott, Oleg; Olson, Arthur J. *Journal of Computional Chemistry*, **31**, 455-461.

Vlaminck, L., De Rouck, B., Desmet, S., Van Gerrewey, T., Goeminne, G., De Smet, L., Storme, V., Kyndt, T., Demeestere, K., Gheysen, G., Inze, D., Vanholme, B. and Depuydt, S. (2022) Opposing effects of trans- and cis-cinnamic acid during rice coleoptile elongation. *Plant Direct*, **6**, e465.

Westfall, C.S., Sherp, A.M., Zubieta, C., Alvarez, S., Schraft, E., Marcellin, R., Ramirez, L. and Jez, J.M. (2016) Arabidopsis thaliana GH3.5 acyl acid amido synthetase mediates metabolic crosstalk in auxin and salicylic acid homeostasis. *Proc Natl Acad Sci U S A*, **113**, 13917-13922.

Zhang, Z., Li, Q., Li, Z., Staswick, P.E., Wang, M., Zhu, Y. and He, Z. (2007) Dual regulation role of GH3.5 in salicylic acid and auxin signaling during Arabidopsis-Pseudomonas syringae interaction. *Plant Physiol*, **145**, 450-464.

FIGURES

Table 1. PA is conjugated by the plant.

Metabolic profiling was performed for etiolated mock-treated Col-0, PA-treated Col-0 and *c4h-4* seedlings (El Houari *et al.*, 2021b) after transfer to the light for 7 days. The table shows the top 15 accumulating compounds and their average peak area ± SE for PA-treated seedlings compared with *c4h-4* seedlings (n>7) for all 3 conditions (mock-treated Col-0 (WT), PA-treated Col-0 and *c4h-4* seedlings). For each of these compounds a number (No.), mass-to-charge ratio (*m/z*) and retention time (RT) is given.

No.	RT	*m/z*	Name	WT	*c4h-4*	PA
1	5.64	280.0457	Piperonyl aspartate	0.00 ± 0.00	3.00 ± 8.21	9085.10 ± 2990.26
2	6.49	294.0613	Piperonyl glutamate	0.00 ± 0.00	0.00 ± 0.00	2176.32 ± 895.68
3	9.04	753.1494	Unknown	0.00 ± 0.00	0.00 ± 0.00	1001.24 ± 440.91
4	5.80	327.0711	Piperonyl hexose	0.00 ± 0.00	1.00 ± 1.54	710.03 ± 250.90
5	4.84	293.0772	no MS/MS	2.00 ± 0.59	0.00 ± 0.00	576.88 ± 238.47
6	5.26	407.0281	Piperonyl sulfohexose	0.00 ± 0.00	0.00 ± 0.00	531.41 ± 215.38
7	9.51	380.9547	no MS/MS	0.00 ± 0.00	0.00 ± 0.00	473.64 ± 161.19
8	5.63	236.0553	Piperonyl aspartate fragment	0.00 ± 0.00	0.00 ± 0.00	380.09 ± 128.55
9	5.78	165.019	Piperonyl hexose	0.00 ± 0.00	0.00 ± 0.00	349.51 ± 78.97
10	5.62	379.9698	Unknown	0.00 ± 0.00	0.00 ± 0.00	345.08 ± 92.89
11	9.52	165.019	PA	0.00 ± 0.00	0.00 ± 0.00	298.39 ± 82.70
12	5.77	363.047	Unknown	0.00 ± 0.00	0.00 ± 0.00	261.41 ± 95.63
13	4.61	535.1293	PA + 2 hexoses	0.00 ± 0.00	0.00 ± 0.00	247.16 ± 117.25
14	9.05	827.1488	no MS/MS	0.00 ± 0.00	0.00 ± 0.00	209.75 ± 190.79
15	9.50	615.9776	no MS/MS	0.00 ± 0.00	0.00 ± 0.00	204.78 ± 78.18

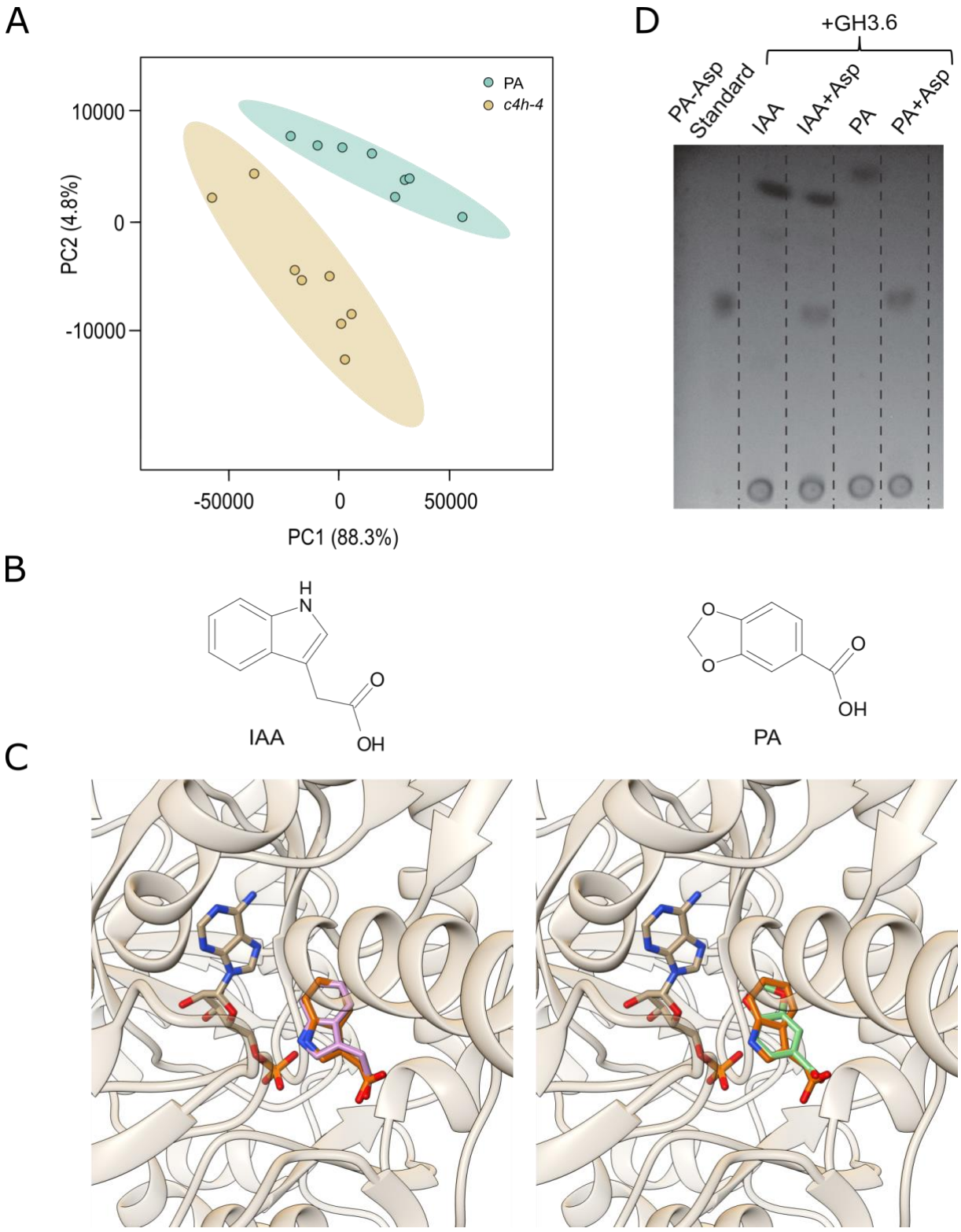

Figure 1. PA is recognized and conjugated by GH3.6.

(A) Principal component analysis score plots for the metabolic profiles obtained by

LC-MS analysis of etiolated *c4h-4* and 50 µM PA-treated Col-0 seedlings (n=8) after transfer to the light for 7 days. Each data point represents eight pooled seedlings. (B) Chemical structures of IAA and PA. (C) Docking of the best possible position for IAA (left, pink) and PA (right, green) in the modeled GH3.6 binding pocket. The experimentally determined position of IAA (orange) and adenosine monophosphate is shown for both figures. (D) TLC analysis of the products of *in vitro* enzymatic assays by GH3.6 supplemented with IAA (1mM) ± Asp (2mM) and PA (10mM) ± Asp (2mM). A standard for PA-Asp was included (left).

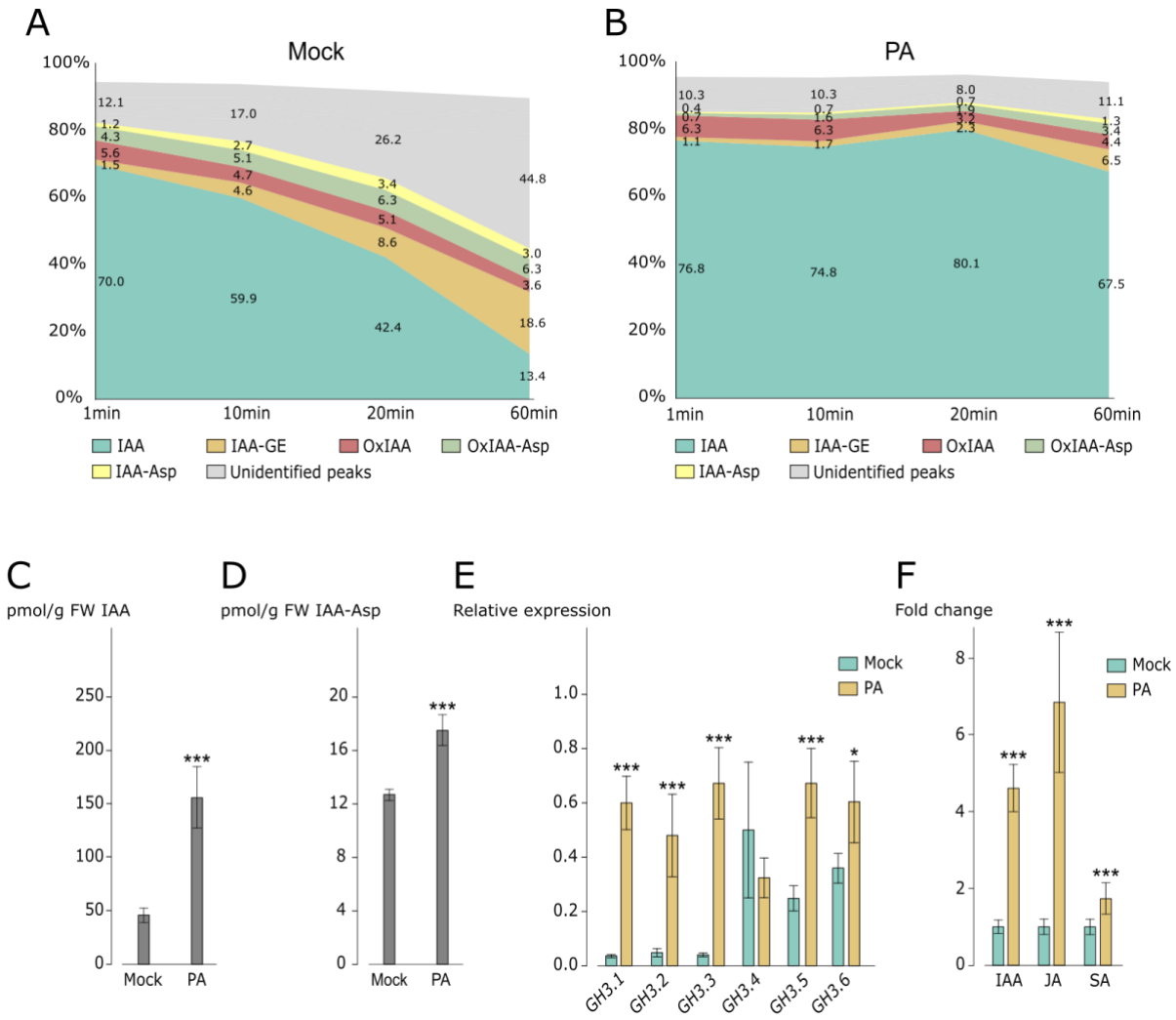

Figure 2. Conjugation of PA impacts phytohormone homeostasis.

(A-B) Quantification of IAA and IAA conjugates in BY-2 cells over time upon addition of ^{3}H-IAA and treatment without (A) or with (B) PA (n=4). (C-D) Quantification of IAA (C) and IAA-Asp (D) in etiolated seedlings treated with or without 50 µM PA (n=10) after transfer to the light for 7 days. Error bars represent 95% confidence intervals. Asterisks are given to distinguish statistically significant values (***:P<0.0001; Student's t-test). (E) Expression levels of *GH3.1-6* in mock-treated and PA-treated in etiolated seedlings (n=9) after transfer to the light for 7 days. Error bars represent 95% confidence intervals. Asterisks indicate significant differences compared to the corresponding mock-treatment (*:P<0.01; **:P<0.001; ***:P<0.0001; Student's t-test) (F) Quantification of IAA, JA and SA in etiolated seedlings treated with or without 50 µM PA (n=9) after transfer to the light for 7 days. Error bars represent 95% confidence intervals. Asterisks are given to distinguish statistically significant values (***:P<0.0001; Student's t-test).

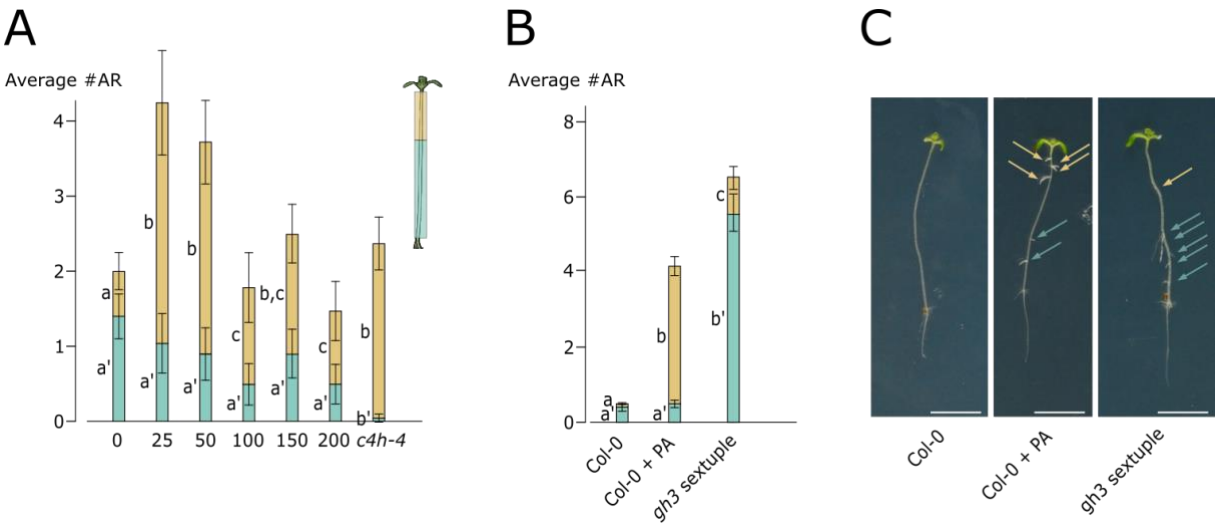

Figure 3. Obstructing the function of GH3s results in increased adventitious rooting

(A) Average number of ARs of etiolated PA-treated (0-200 µM) and *c4h-4* mutant seedlings (n>25) after transfer to the light for 7 days. Error bars represent 95% confidence intervals. Letters a-c and a'-b' are given to distinguish statistically significant results (P<0.05; General Estimation Equation (GEE) model). (B) Average number of ARs of etiolated mock- and PA-treated Col-0 seedlings and *gh3* sextuple (*gh3.1-6*) mutant seedlings (n>90) after transfer to the light for 7 days. Error bars represent 95% confidence intervals. Letters a-c and a'-b' are given to distinguish statistically significant results (P<0.05; GEE model). (C) Representative phenotypes for etiolated mock- and PA-treated Col-0 seedlings and *gh3* sextuple mutant seedlings after transfer to the light for 7 days. Yellow arrow, ARs located in the top third part of the hypocotyl; blue arrow, ARs located at the bottom two-thirds part of the hypocotyl. Bar = 1cm.

SUPPLEMENTAL TABLES & FIGURES

Supplemental table S1. Primers used for qPCR analysis

Gene	Locus	Primer_FW	Primer_REV
ACTIN2	AT3G18780	TTGACTACGAGCAGGAGATGG	ACAAACGAGGGCTGGAACAAG
ACTIN7	AT5G09810	TCCATGAAACAACTTACAACTCCATCA	CATCGTACTCACTCTTTGAAATCCACA
UBQ10	AT4G05320	GGCCTTGTATAATCCCTGATGAATA	AAAGAGATAACAGGAACGGAAAC
GH3.1	AT2G14960	CTCGGTGCTGCTTGGAAATG	TGGGCTGAAGTGTGTAGATA
GH3.2	AT4G37390	CTTAGACCGACGTCAGCTTTTATACAG	GGTAACCCACCTGACGTCTTTG
GH3.3	AT2G23170	ACGTCAGCTTTTATACAGTCT	GCTGGTAATCCACCGGGAGTCT
GH3.4	AT1G59500	ACTTCAGGACGTCGGATTCA	TTTGAGACGAGTCACAGCAGA
GH3.5	AT4G27260	GCTTGTTGTCACCACTTACGCC	GCTTTGTTCTTGAAACCAGTCACTC
GH3.6	AT5G54510	CTATCAGTCTTCCAAAAGCACTCAC	TTCTTGAAACCAGCCACGC

Supplemental table S2. Quantification of IAA and IAA conjugates upon treatment with or without PA.

Quantification of IAA and IAA conjugates in BY-2 cells over time upon addition of ^{3}H-IAA and treatment without or with PA (n=4).

Mock

Peak no.	Peak ID	RT (min)	1 min	10 min	20 min	60 min
1	Background					
2	-	3.35	0.80 ± 0.24	6.72 ± 1.17	14.48 ± 2.13	34.21 ± 1.46
3	-	4.92	0.43 ± 0.09	1.50 ± 0.15	2.83 ± 0.24	6.15 ± 0.60
4	OxIAA-Asp	6.92	4.25 ± 0.80	5.13 ± 0.33	6.28 ± 0.51	6.25 ± 0.32
5	IAA-Asp	9.30	1.18 ± 0.13	2.65 ± 0.17	3.42 ± 0.14	3.05 ± 0.06
6	OxIAA	10.12	5.63 ± 1.14	4.65 ± 0.14	5.08 ± 0.63	3.61 ± 0.42
7	IAA-GE	13.30	1.46 ± 0.03	4.59 ± 0.29	8.64 ± 0.20	18.60 ± 1.10
8	IAA	15.98	69.96 ± 3.06	59.90 ± 1.79	42.38 ± 4.20	13.39 ± 0.91
9	-	18.67	2.52 ± 0.48	1.87 ± 0.05	1.91 ± 0.26	1.28 ± 0.13
10	-	23.62	3.87 ± 0.44	3.09 ± 0.32	2.62 ± 0.16	1.09 ± 0.18
11	-	24.98	4.43 ± 0.69	3.86 ± 0.20	4.36 ± 0.87	2.05 ± 0.14

+PA

Peak no.	Peak ID	RT (min)	1 min	10 min	20 min	60 min
1	Background					
2	-	3.35	0.34 ± 0.12	1.06 ± 0.15	1.22 ± 0.28	3.38 ± 0.44
3	-	4.92	0.22 ± 0.10	0.26 ± 0.06	0.26 ± 0.06	0.61 ± 0.13
4	OxIAA-Asp	6.92	0.73 ± 0.07	1.62 ± 0.19	1.93 ± 0.15	3.45 ± 0.23
5	IAA-Asp	9.30	0.39 ± 0.03	0.74 ± 0.07	0.73 ± 0.08	1.25 ± 0.08
6	OxIAA	10.12	6.34 ± 0.90	6.34 ± 0.77	3.22 ± 0.67	4.36 ± 0.74
7	IAA-GE	13.30	1.05 ± 0.14	1.73 ± 0.17	2.30 ± 0.09	6.53 ± 0.15
8	IAA	15.98	76.80 ± 2.95	74.76 ± 2.25	80.12 ± 1.59	67.51 ± 2.62
9	-	18.67	2.54 ± 0.10	2.32 ± 0.28	1.26 ± 0.15	1.43 ± 0.33
10	-	23.62	3.52 ± 0.12	3.26 ± 0.21	2.81 ± 0.39	2.80 ± 0.14
11	-	24.98	3.69 ± 1.19	3.40 ± 0.30	2.40 ± 0.50	2.86 ± 0.31

Supplemental figure S1. List of MS/MS spectra used for characterization of compounds in table 1.

Except for PA, all compounds were structurally characterized based on their *m/z* and MS/MS. PA was characterized based on *m/z* and retention time match with its chemical standard.

1. Piperonyl aspartate (*m/z* 280.0457; 5.64 min.)

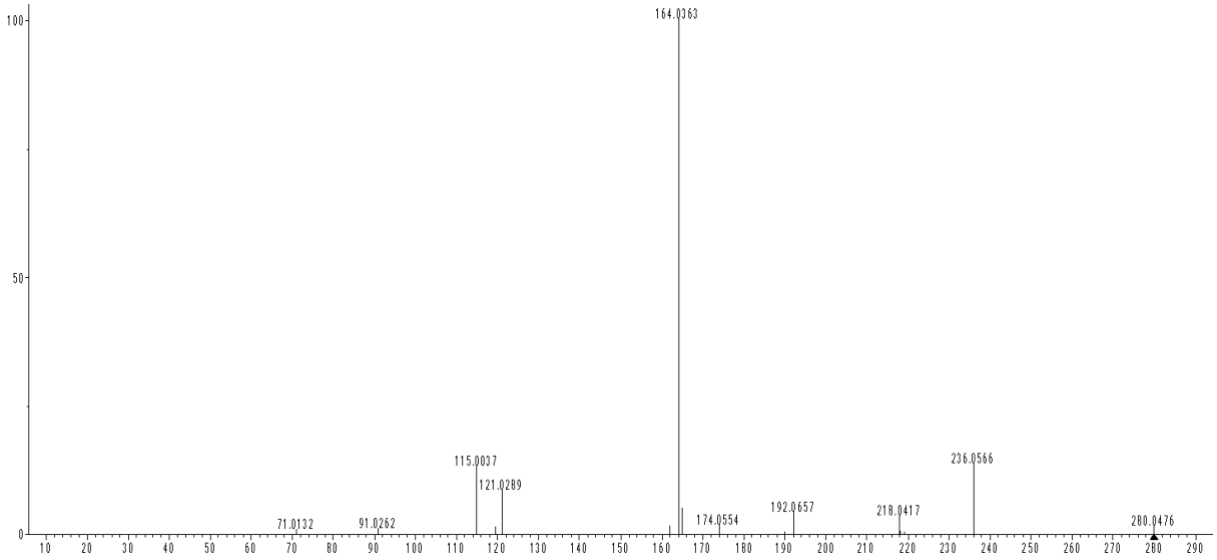

2. Piperonyl glutamate (*m/z* 294.0613; 6.49 min.)

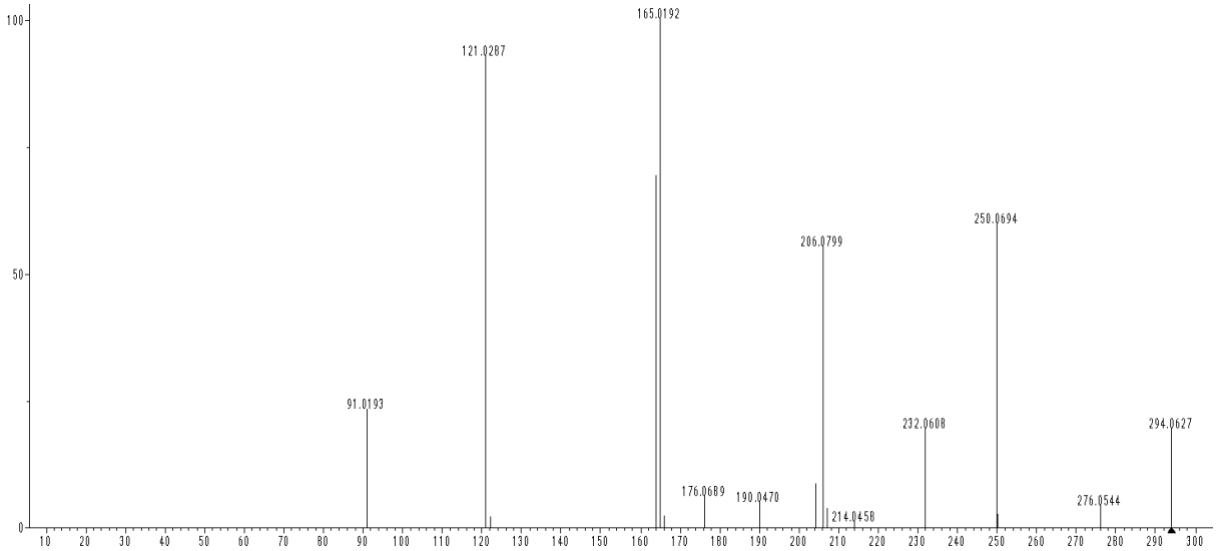

3. Unknown (*m/z* 753.1494; 9.04 min.)

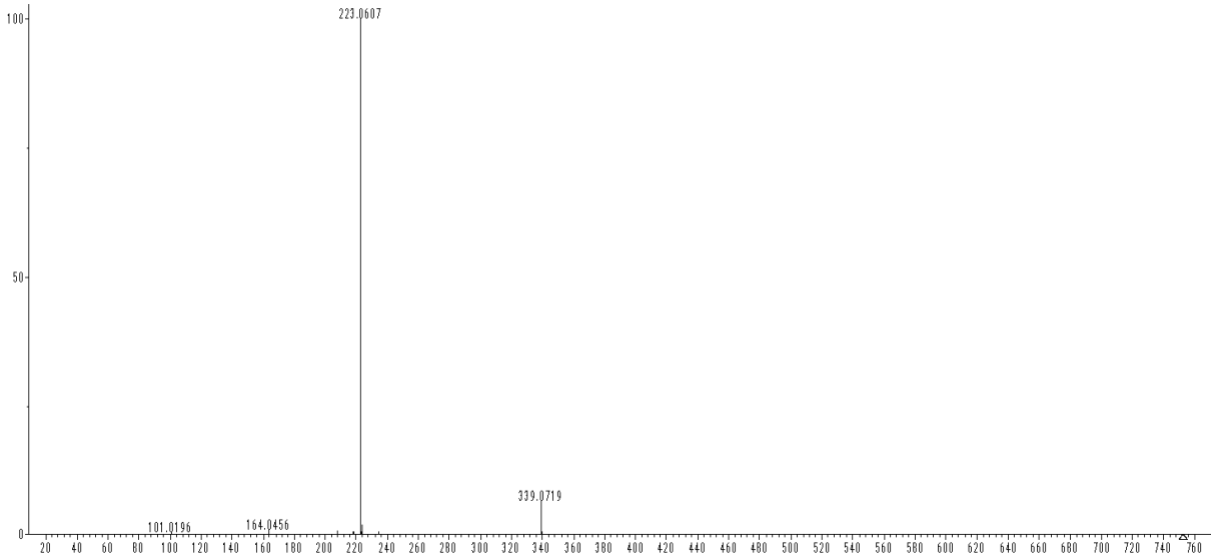

4. Piperonyl hexose (*m/z* 327.0711; 5.80 min.)

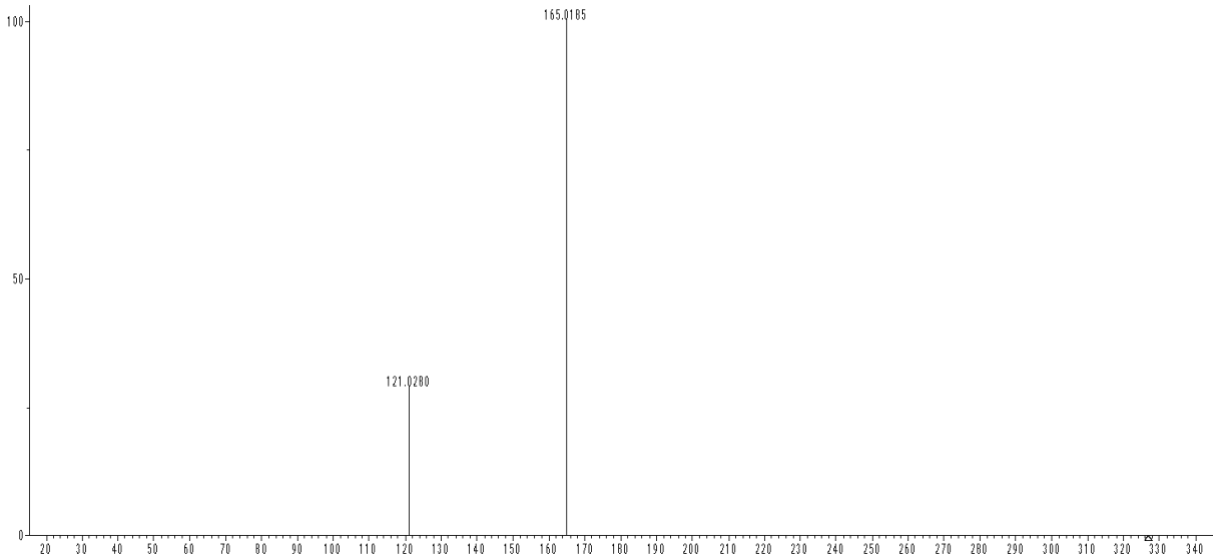

6. Piperonyl sulfohexose (*m/z* 407.0281; 5.26 min.)

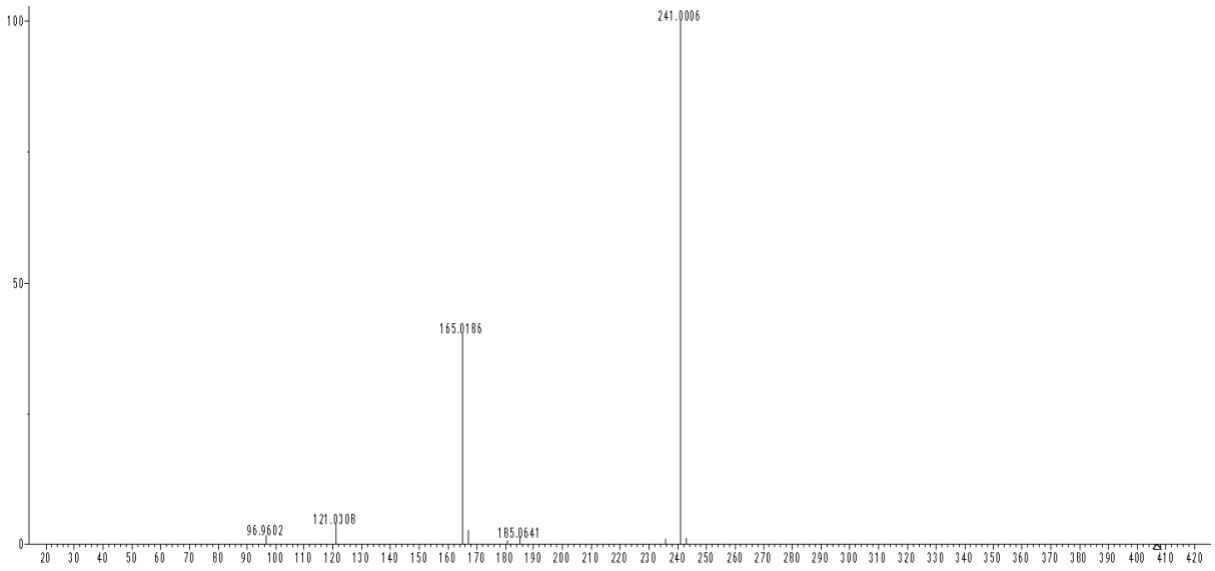

8. Piperonyl aspartate fragment (*m/z* 236.0553; 5.63 min.)

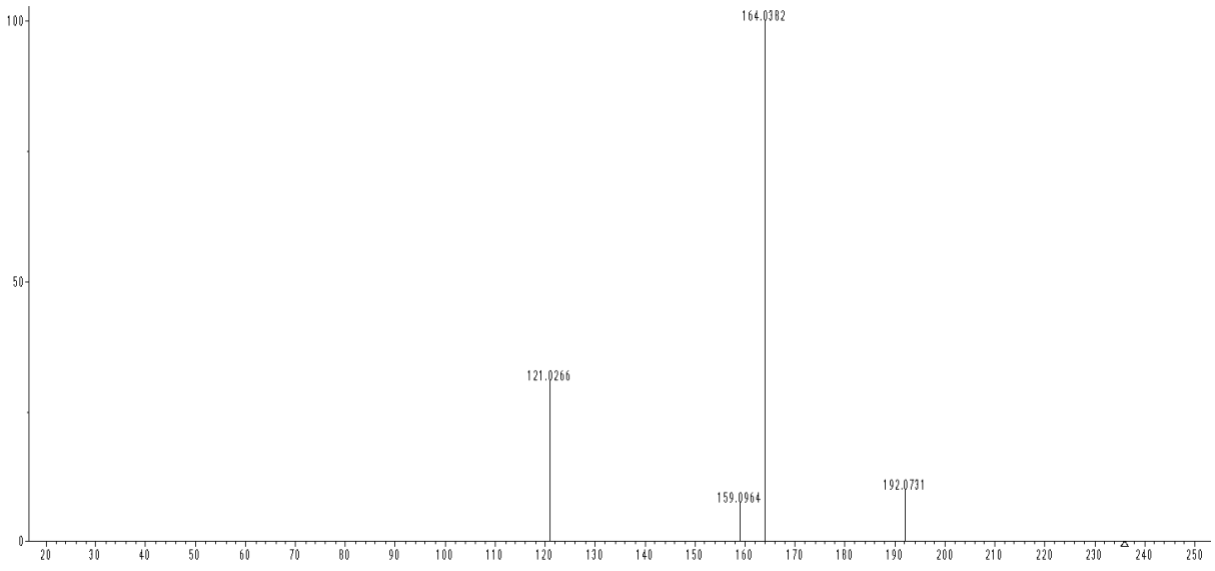

9. Piperonyl hexose (*m/z* 165.019; 5.78 min.)

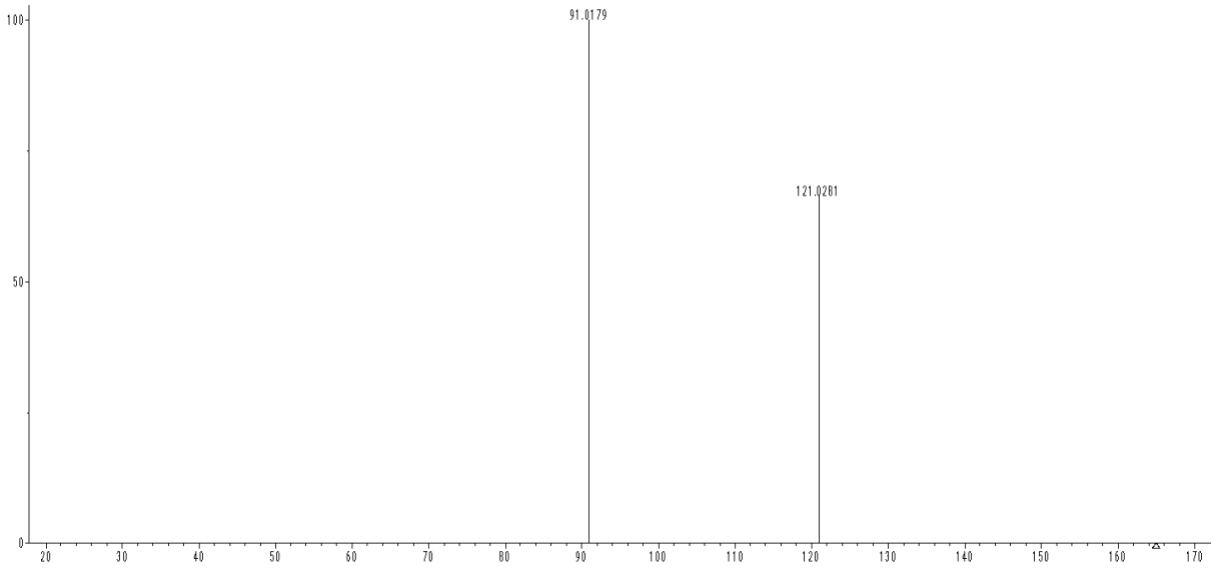

10. Unknown (*m/z* 379.9698; 5.62 min.)

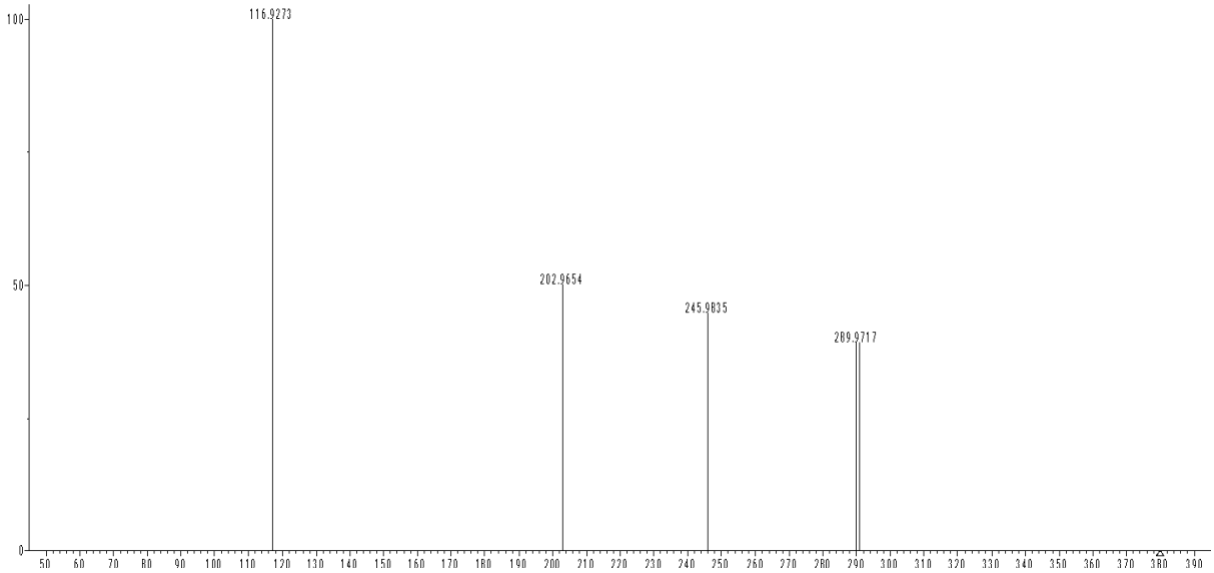

11. PA (*m/z* 165.019; 9.52 min.)

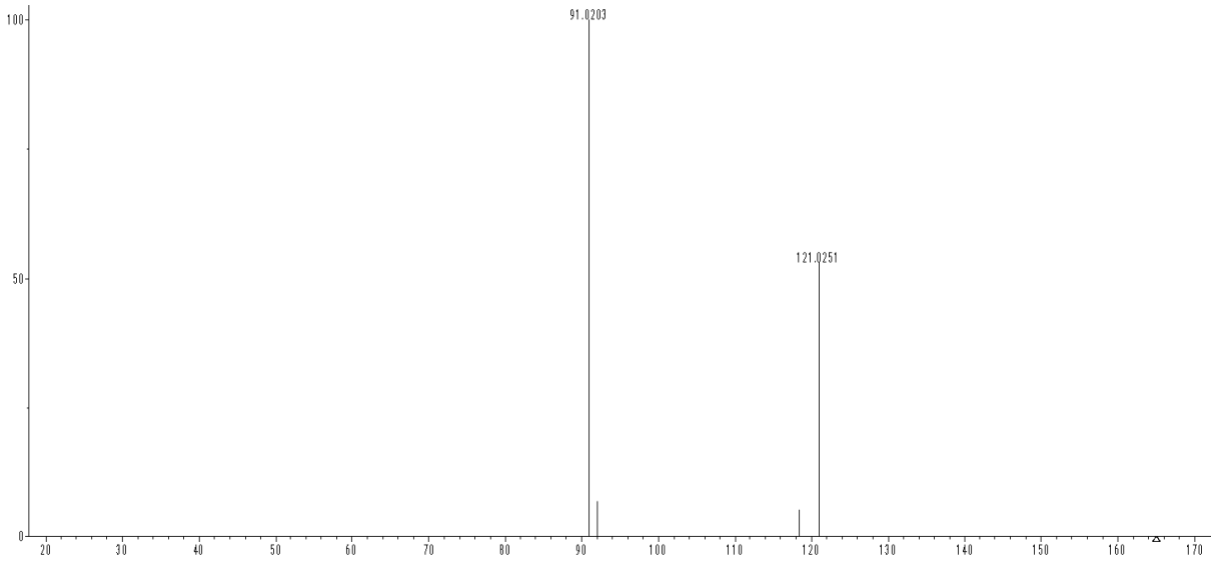

12. Unknown (*m/z* 363.047; 5.77 min.)

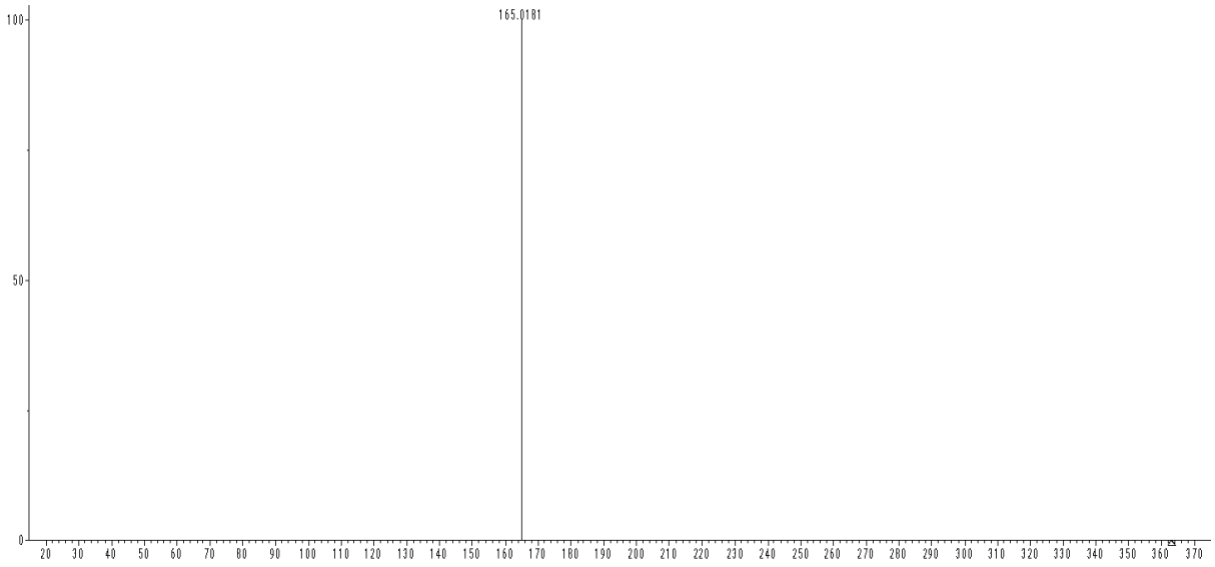

13. PA + 2 hexoses (*m/z* 535.1293; 4.61 min.)